Journal of Inorganic and Organometallic Polymers and Materials (2020) 30:4106–4116
https://doi.org/10.1007/s10904-020-01564-z

Single and Multi-metal Oxide Nanoparticles Induced Cytotoxicity and ROS Generation in Human Breast Cancer (MCF-7) Cells

Maqsood A. Siddiqui[1,2] · Rizwan Wahab[1,2] · Javed Ahmad[1,2] · Nida N. Farshori[3] · Abdulaziz A. Al-Khedhairy[1]

Received: 17 February 2020 / Accepted: 25 April 2020 / Published online: 4 May 2020

Abstract
The present study was designed to examine the cytotoxic activity of synthesized single metal oxide nanoparticles such as copper oxide (CuO), iron oxide (γFe_2O_3) and multi-metal oxide zinc, iron and copper oxide ($CuZnFe_2O_3$) in human breast cancer (MCF-7) cells. These single and multi-metal oxide nanoparticles were characterized by X-ray diffraction (XRD) and scanning electron microscopy (SEM). The cytotoxic potential of these nanoparticles was assessed by MTT and NRU assays. Further, the morphological alterations, reactive oxygen species (ROS) generation and mitochondrial membrane potential (MMP) were also studied. The novelty of the present work express that the MTT and NRU assays revealed a concentration dependent decrease in the viability of MCF-7 cells. The percent cell viability was recorded as 82%, 81%, and 79% in CuFeZn NPs, 81%, 80% and 70% in γFe_2O_3NPs, 54%, 43% and 27% in CuONPs exposed MCF-7 cells for 24 h at doses 25, 50, 100 µg/ml, respectively by MTT assay. The MTT results was also justified by NRU assay. An increase in ROS generation was observed as 21% and 35% in CuOFeZnNPs, 41% and 61% in γFe_2O_3NPs and 54% and 89% in CuONPs and the decrease in MMP level was observed as 14% and 24% in CuOFeZn NPs, 37% and 46% in γFe_2O_3NPs and 52% and 58% in CuONPs at 25 and 50 µg/ml, respectively related to control. Together, these results suggest that the loss of MMP and increase in ROS level could be important mechanism of single and multi-metal oxide nanoparticles induced cytotoxicity in human breast cancer cells.

Keywords Metal oxide nanoparticles · Cytotoxicity · MCF-7 cells · ROS generation · Mitochondrial membrane potential

1 Introduction

The field of nanomaterial (NM) has become an ever-growing discipline of science of the entire world because it exhibits unique quantum size effect. In modern era, NMs received great attention among researchers since of their promising applications in a huge diversity of fields. These NMs have property to improve the electronic, magnetic, mechanical, chemical, enhanced nonlinear optical and surface properties, are inherently different from both their corresponding atoms, molecules and could be used as catalysts, ferrofluids, data storage, biomarkers, sensors, bio-sensors, color imaging, pigments and in ceramics [1–5]. Similarly, consolidated nanophase materials also exhibit properties different from those of conventional bulk materials and found to have improved mechanical properties [6, 7]. For decades, among the nanomaterials chemists and materials scientists are very keen to create metal oxides (MOs) and mixed metal oxides (MMOs) nanostructures for both unique properties and technological utilities for instance electronic, magnetic and synergetic stuffs [8, 9]. Oxides including transition metals and rare earths, display a very wide variety of complex structures and their interesting properties. These MMOs (such as zinc oxide with various metals; copper zinc ferrite, copper oxide with other metals (copper iron oxide, cobalt oxide, cobalt nickel oxide, cobalt iron oxides etc.) can greatly generate new synergetic properties and improve overall application performance by due to wide band gap and appropriate combination of individual oxide components [10]. These MMOs are increasingly being used for the

✉ Rizwan Wahab
rwahab@ksu.edu.sa; rwahab05@gmail.com

1 DNA Research Chair, Zoology Department, College of Science, King Saud University, P.O. Box 2455, Riyadh 11451, Saudi Arabia

2 Zoology Department, College of Science, King Saud University, P.O. Box 2455, Riyadh 11451, Saudi Arabia

3 Department of Pharmacognosy, College of Pharmacy, King Saud University, Riyadh 11451, Saudi Arabia

remediation and drug delivery purposes [11, 12]. Numerous ways can be used for the preparation of nano structured of MMOs such as co-precipitations, sol–gel processes, solvothermal techniques, microemulsion, combustion, vapor condensation, spray pyrolysis, template and surface derivatized methods [13]. The preparation method of MMOs can have a critical influence on the morphology of resulting material, and consequently affect the technological applications. Very limited reports have been published on the synthesis of MMOs nanocomposite. Enroute to this, the synthesis of core of Cu_2S wrapped-up with thin layer of TiO_2-shell was fabricated and applied for the photo-excitons for H_2 production [14]. The mixed oxides gadolinium substituted bismuth ferrite ($BiFeO_3$) was synthesized and examine their photocatalytic and bio sensing properties. The received data implies that the BF materials improve the bio-sensing properties with detected through cyclic voltammogram technique [15]. The oxide metal, doped and template free oxides shows much sensing characteristic for their biomedical, energy storage and water treatment applications [16, 17]. The zinc oxide nanostructures also utilized as sensor material with three electrode system for to quantify drugs (such as antihistamine drug, methdilazine (MDH)) analyzed via cyclic voltammetry (CV) [18]. The TiO_2 nanoparticles, which is an excellent semiconductor utilized for the development and miniaturization of bio sensor devices in the form of hybrids-based biosensors for numerous biological markers applied for healthcare systems [19]. The TiO_2 is also widely utilized for energy purposes such as photocatalytic, hydrogen storage, solar cells etc. [20]. The Cu_2O-coated multi-walled carbon nanotubes (MWCNTs) were synthesized from the Fehling's reagent and characterized for the catalysis and optoelectronic applications [21]. Including other types of materials, the doped (Y) and co-doped (Cu, Y) with Hematite (α-Fe_2O_3) is the finest material for water oxidation [22]. Iron (Fe)-doped ZrO_2 tetragonal like structures was synthesized via hydrothermal process and for to achieve maximum photocurrent density, highest stability via catalytic and electrochemical determination [20, 23–25]. The different metal oxides were utilized in various biomedical purposes such as ZrO_2 coated with liquid metals forms a core–shell nanostructure for photothermal and vehicle for nano-theranostics properties [26]. In another report, copper nanoparticles were prepared from the Green synthesis with *Tinospora cardifolia* and utilized as a nano-fabric for the anti-microbial activity and more than 100% efficiency was achieved [27]. The pH sensitive biological polymer network was developed with using polyacrylamide-g-locust bean gum (PAAm-g-LBG) in combination with sodium alginate for the delivery of ketoprofen [28]. In continuation, the biopolymers gels were also utilized for the ocular testing's [29]. The pyrimidine polymers derivatives such as 1,5-benzodiazepines were obtained from one pot synthesis approach and applied against their antibacterial evaluation [30]. The lipid based lipid-polymer hybrid nanoparticles (LPHNs) also utilized for the drug delivery purposes.

The hybrid nanopolymers can facilitates to optimize the size of nanoparticles, holding drugs, surface functional properties with various biological materials (antibody, peptides, aptamers etc.) also released the drug in blood for longer period [31]. The nano and nano related object have great impact and high potential to deal numerous characteristics of bone malignancies [32]. Over other forms of utilization of nano based materials in various biological applications, the nanoparticles are largely applied against cancer treatment and as an antimicrobial agent [33, 34]. In previous, the MMOs were prepared with the use of expensive organic chemicals (pyrrole monomer, ammonium persulphate, zinc, copper and iron oxide) via in-situ polymerization method [35]. In other reports, the multi metal oxide based nanomaterials were utilized to examine the probable of NMs for the genotoxic *in vitro* and *in vivo* mammalian study [36, 37]. The plenty of work had been published on single metals such as ZnO, CuO, Fe_2O_3, TiO_2 etc. in almost all single metal shows the toxicity whereas the MMOs exhibit a gentle effect on cells population and not to direct damage their cell walls [38–40]. In our case we have used inexpensive and very easy solution process to from the good quality nanostructures and were utilized against breast cancer cells (MCF-7) and have very limited studies are available on interaction of MMOs.

Here, we focused on the preparation of MMOs using solution/precipitation technique to study their characterization and cytological study. Our prime objective for the present work is to investigate the efficacy on MCF-7 cells and their cytotoxic effect through various spectroscopic techniques. In this manuscript, the prepared single and multi-oxides (MMOs) were utilized to know their comparative study against cancer cells.

2 Materials and Methods

2.1 Experimental

2.1.1 Formation of Copper Oxide Nanoparticles (CuONPs)

The synthesis of CuO-NPs was performed with consuming monohydrate of copper acetate (Cu $(CH_3COO)_2{\cdot}H_2O$), *n*-propyl amine (CH_3–$(CH_2)_2$–NH_2) with NaOH purchased from Aldrich chemical corporation USA, received in Riyadh, Saudi Arabia and used as received. In a typical experiment: copper acetate hydrate (0.3 M) and *n*-propyl amine were assorted with 1:5 ratio in 100 ml methanol (MeOH) with constant stirring in a beaker. To this transparent blue colored solution, NaOH (0.1 M), mixed and shaked each time for complete mingling. Thereafter, solutions pH (cole parmer,

USA) was examined and due to increased basicity of the solution, pH was reached upto 12.01. Afterward, the prepared solution was moved in a refluxing pot (~250 ml capacity) and refluxed at ~90 °C for 6 h. The colour of the solution (blue) was changes (black), when the temperature reached to their optimal position. The formed product was centrifuged (3000 rpm for 3 min, Eppendorf, 5430R, Centrifuge, Germany) and re-suspended and washed with ethanolic (EtOH), acetone repeatedly to remove the ionic impurities. Room temperature drying was adopted for the prepared material and utilized for further studies.

2.1.2 Formation of Iron Oxide Nanoparticles (γFe_2O_3NPs)

The synthesis of γFe_2O_3were performed with using iron nitrate nonahydrate ($Fe(NO_3)_3{\cdot}9H_2O$), *n*-propyl amine ($CH_3–(CH_2)_2–NH_2$) purchased from Aldrich chemical corporation USA, received in Riyadh, Saudi Arabia and used as without further purification. In an typical experiment: $Fe(NO_3)_3{\cdot}9H_2O$ (0.3 M) and propyl amine were mixed with the same ration (1:5) as stated above in methanol (MeOH) solvent under stirring (~30 min), the colour of solution was brown at time which seemed in a beaker. To this colored solution, NaOH (0.1 M), was mixed and shaked each time for complete mingling. Then after solutions pH was measured which elevated to 12.06. This solution was transferred to a glass pot and refluxed same temperature and time as sated above (at ~90 °C for 6 h). With the increase of solution temperature, the colour of solution (light brown) also changes to dark brown colour. The reaction process was stopped at fixed time and obtained product cooled to room temperature and centrifuged (3000 rpm for 3 min, Eppendorf, 5430R, Centrifuge, Germany), again re-suspended in alcohol (MeOH, EtOH) and acetone and washed to remove impurities from formed product. The product was dried at room temperature and used for further studies.

2.1.3 Formation of CuZnFe Oxide Nanoparticles

The formation of mixed metal (CuZnFe Oxide) oxide nanoparticles were performed with using, equimolar concentration (0.3 M) of metal precursor salts such as zinc acetate di-hydrate ($Zn(CH_3COO)_2{\cdot}2H_2O$), copper acetate hydrate ($Cu(CH_3COO)_2{\cdot}H_2O$) and iron nitrate hydrate ($Fe(NO_3)_3{\cdot}9H_2O$) were chosen and dissolve in a methanol (MeOH, 300 ml) solvent and stirred under constant stirring for 30–40 min and dissolved, a desired ratio 1:5 of propyl amine was incorporated to this mixture. To this solution sodium hydroxide (NaOH, 0.1 M) was added as drop by drop, to increase the basicity of the reaction and solution pH was examined and it reaches upto 12.61. The obtained product was moved in a refluxing pot and refluxed with the same temperature and time as stated above. Red coloured precipitate was obtained in the refluxing pot after the complete refluxing time. Washed the obtained product with alcohol (MeOH, EtOH) and acetone repeatedly and dried at room temperature and to keep for further studies.

2.2 Materials Characterization

The phase, crystallinity and size of the prepared nanostructures were characterized by the X-ray diffraction pattern (XRD, Rigaku, Japan) with $Cu_{K\alpha}$ radiation ($\lambda = 1.54178$ Å) in the range of 20°–80° with 6°/min scan speed in accelerating voltage of 40 kV and current was 30 mA. The structural evaluation was measured via scanning electron microscopy (SEM, JEOL 6380, JSM Japan). For the SEM analysis of prepared nanostructures powder was sprinkled on carbon tape and the unwanted material was eliminated from the air blower. The sample holder was transfer in a specialized glass chamber and sputtered with platinum (~3 *s*). After sputtering sample holder was fixed in SEM and analyzed the samples at room temperature.

2.3 Biological Studies

2.3.1 Culture Medium and Consumables

Dulbecco's modified eagle's medium (DMEM), antibiotics/antimycotics solution and fetal bovine serum (FBS) were purchased from sigma company, USA. Culture wares and specified chemicals/reagents were purchased from Nunc and Sigma, respectively.

2.3.2 Culture of Cell Line

MCF-7, a human breast adenocarcinoma cell line was cultured in DMEM with 10% FBS, 0.2% sodium bicarbonate, and antibiotic/antimycotic solution. Cells were grown in a CO_2 incubator at 37 °C. The viability of cells was assessed by trypan blue dye test [41] prior to the experiments. The cells showing more than 98% viability were used in present study.

2.3.3 MTT Assay

The MTT (3-(4,5-dimethylthiazol-2-yl)-2,5-diphenyl tetrazolium bromide) assay was performed using the protocol of Siddiqui et al. [42]. For this assay, MCF-7 cells (1×10^4 cells) were plated in 96 well plates and kept for adherence overnight in a CO_2 incubator. The MCF-7 cells were exposed to CuFeZn NPs, γFe_2O_3NPs and CuONPs at 1–100 µg/ml for 24 h. After the exposure, 10 µl/well of MTT solution (5 mg/ml) was added in 100 µl of medium and kept plates in incubator for 4 h. The supernatant was then removed and DMSO

(200 µl) was added in each well and pipette to dissolve the crystal. The absorbance was read at a wavelength of 550 nm.

2.3.4 Neutral Red Uptake Assay

To assess the cytotoxic potential of CuFeZnNPs, γFe_2O_3NPs and CuONPs, the NRU assay was also done as per the protocol described [43]. In brief, MCF-7 cells (1×10^4) were plated in 96 well plates and kept for adherence overnight in a CO_2 incubator. Then cells were exposed to CuFeZn NPs, γFe_2O_3NPs and CuONPs at 1–100 µg/ml for 24 h. After the exposure, 50 µg/ml of NR dye containing culture medium was added in each well. The cells were then subjected to 3 h of incubation. Then, the wells were washed with a solution of 0.5% CH_2O and 1% $CaCl_2$. Further, a solution of 1% CH_3COOH and 50% EtOH was added and the dye was extracted. The absorbance was then read at a wavelength of 550 nm.

2.3.5 Cell Morphology

CuFeZnNPs, γFe_2O_3NPs and CuONPs induced alterations in the morphology of MCF-7 exposed to 1–100 µg/ml for 24 h was observed under the phase contrast inverted microscope. The images were grabbed at 20× magnification.

2.3.6 Induction in ROS Production

The induction in ROS production in MCF-7 cells exposed to CuFeZnNPs, γFe_2O_3NPsand CuONPs for 24 h was observed using fluorescence dye (2,7-dichlorodihydrofluorescein diacetate (DCFH-DA; Sigma Aldrich, USA) [44]. Following exposure of CuFeZnNPs, γFe_2O_3NPsand CuONPs, test solution was removed. After washing with PBS, MCF-7 cells were exposed to DCFH-DA (20 µM) for 1 h at 37^0C in dark. 60 min. The fluorescence intensity of the dye in cells was visualized under fluorescence microscope.

2.3.7 Change in Mitochondrial Membrane Potential

The decrease in MMP level was assessed using the method of Siddiqui et al. [44]. In brief, cells were exposed to 25–100 µg/ml of CuFeZnNPs, γFe_2O_3NPsand CuONPs for 24 h. After washing the exposed and unexposed cells twice with PBS, cells were exposed to 10 µg/ml of fluorescence dye (Rhodamine-123) at 37 °C in dark for 60 min. Further, cells were washed twice with PBS and fluorescence of Rh-123 dye was visualized under fluorescence microscope. The images of cells were grabbed at 20× magnification.

2.3.8 Statistical Analysis

The significance differences between exposed and control groups were analyzed using one-way ANOVA and post-hoc Dunnett's test. The values depicting $p < 0.05$ were considered as statistically significant.

3 Results

3.1 X-ray Diffraction Pattern

The crystallinity and phases of the prepared different single and mixed metal oxides NPs were characterized via X-ray diffraction (XRD) pattern (Rigaku, Japan) obtained with $Cu_{K\alpha}$ radiation ($\lambda = 1.54178$ Å) ranges from 20° to 65° with scan speed of 6°/min with an accelerating voltage of 40 kV, and current of 30 mA. Figure 1a shows the XRD pattern of copper oxide NPs synthesized at as described above in material and methods. From the obtained spectra the main indexed peaks obtained at 37.43 ⟨022⟩, 43.63 ⟨202⟩ defines that the prepared material is in crystalline in nature. The XRD pattern shows peaks, which are similar to single crystalline CuO without impurities and well, matched with the standard JCPDS Data Card No. 05-661. Other single metal oxide material iron oxides (γFe_2O_3, Fig. 1b) shows the peaks obtained at 28.98 ⟨220⟩, 37.42 ⟨311⟩ and 43.57 ⟨400⟩ for maghemite are in full agreement with JCPDS Card No. 24-0081. Figure 1c depicts the X-ray diffraction pattern of mixed metal oxides (CuZnFeNPs), which indicates that the indexed peaks obtained at 29.93 ⟨020⟩, 35.11 ⟨313⟩, 42.77 ⟨124⟩, 53.31 ⟨530⟩, 56.5 ⟨240⟩ including one unidentified at 62.15 in the spectrum, are well agreement with JCPDS Card No. 07-0392 and confirms that the prepared NPs are crystalline in nature with their phases. From these

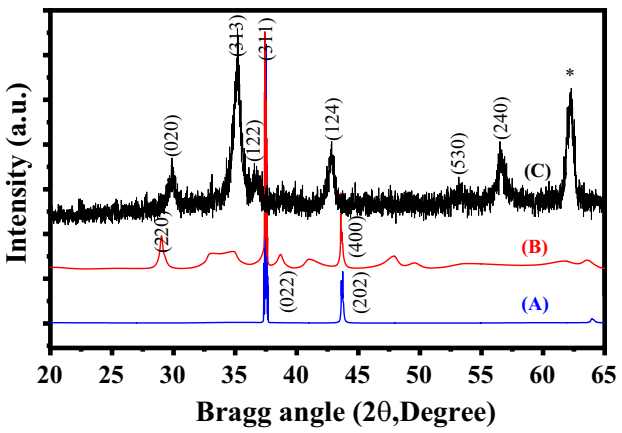

Fig. 1 X-ray different shows the single [CuONPs (**a**) and γFe_2O_3 (**b**)] and multi-metal [CuFeZnNPs, (**c**)] oxides respectively, where * show the unidentified peak in spectra.

spectra it also concluded that there are no other peaks or impurities were accessed in X-ray diffraction with in the detection range, which designates that the prepared materials are pure and crystalline approves that the synthesized powders are pure CuO, Fe_2O_3 and CuZnFeNPs.

3.2 Morphological Analysis [Scanning Electron Microscopy (SEM)]

The structural evaluation of the prepared single and multi-metal nanoparticles was examined with scanning electron microscopy (SEM). The SEM images show the structural evaluation of the prepared three types of nanoparticles. In all morphology of the prepared material exhibits a spherical in shape with an aggregation of other particles. So the material was analyzed at lower and higher magnification ranges (Fig. 2a, b), which shows the synthesized copper oxide (CuONPs) at above described conditions in material and methods, confirmed that the synthesized products are at different sizes. From the acquired data's as images it demonstrates that the average size of each particle as diameter ranges from 45 to 50 nm. The other single metal iron oxides (γFe_2O_3NPs) material low and high magnified images (Fig. 2c, d) were also shows similar morphology with some aggregation. The average size of each nanoparticle is 50 nm in size in spherical in shape. The multi metal material CuZnFe oxide NPs, which shows that some are spherical, ellipsoidal, elongated etc. in shape and have an aggregation which is common for the nanoparticles due to strong interparticle interaction with other particles, the nanoparticles may be the resulted to merge together to form a larger molecule of multi metal nanostructures. The low and high images shows the mixed metal oxide NPs, the size of each nanoparticles is bigger (~ 80 nm) as compared to other single metal oxide nanoparticles, due to the other metal ions (zinc and iron) interaction with parent copper ions in solution (Fig. 2e, f).

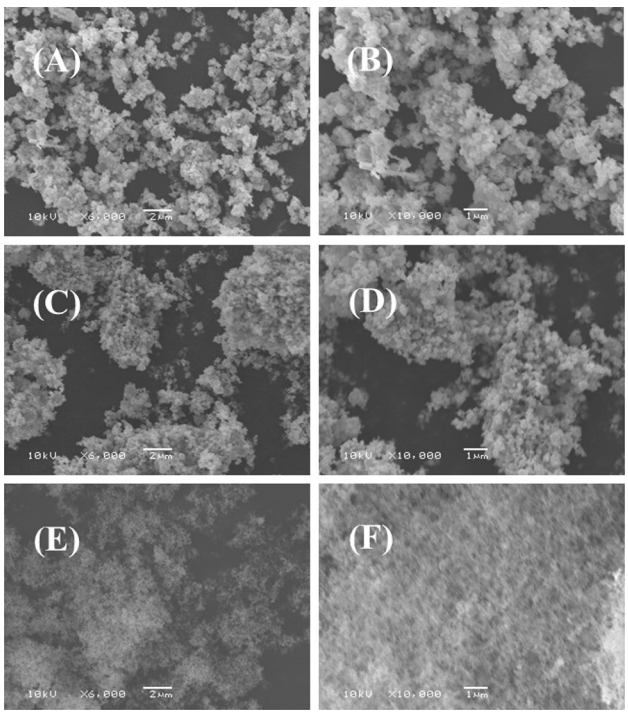

Fig. 2 Low and High magnification scanning electron microscopy images of single and multi-metal oxides: CuONPs (**a**, **b**), γFe_2O_3 (**c**, **d**) and CuFeZnNPs (**e**, **f**) respectively

3.3 MTT Assay

The key results obtained by MTT assay are presented in Fig. 3. After 24 h exposure of CuFeZnNPs, γFe_2O_3NPs and CuONPs induced a dose dependent cytotoxicity in MCF-7 cells. The percent cell viability at 25, 50, and 100 µg/ml was found as 82%, 81%, and 79% in CuFeZnNPs, 81%, 80% and 70% in γFe_2O_3 NPsand 54%, 43% and 27% in CuONPs, respectively in MCF-7 cells (Fig. 3). The MCF-7 cells exposed to CuOFeZnNPs and γFe_2O_3 exhibit less cytotoxicity as compared to CuONPs.

3.4 NRU Assay

The cytotoxic response of CuOFeZn NPs, γFe_2O_3NPs and CuONPs observed by NRU assay are presented in Fig. 4. The MCF-7 cells exposed to 25–100 µg/mL decreased the cell viability in a dose dependent manner. The percent cell viability at 25, 50, and 100 µg/mL was found as 87%, 86% and 76% in CuFeZnNPs, 86%, 78% and 67% in γFe_2O_3 NPs and 69%, 57%, and 39% in CuONPs, respectively in MCF-7 cells. Similar to MTT assay, the MCF-7 cells treated with CuOFeZn NPs and γFe_2O_3NPs exhibited less toxicity as compared to CuONPs (Fig. 4). Our results showed that the lower sized NPs, i.e. CuONPs (45–50 nm) exhibited the highest cytotoxic effects, whereas, γFe_2O_3NPs (50 nm) were moderately cytotoxic and CuFeZnNPs (~ 80 nm) showed least cytotoxic effects in MCF-7 cells exposed for 24 h.

3.5 Morphological Analysis

CuOFeZn NPs, γFe_2O_3NPs, CuO NPs induced alterations in the cell morphology of MCF-7 cells are presented in Fig. 5. As observed under the microscope, the cells showed indicate the most protuberant effects in the morphology of MCF-7 cells after CuOFeZn NPs, γFe_2O_3NPs, CuO NPs exposure for 24 h. At highest dose i.e. 100 µg/ml, the MCF-7 cells lose their typical shape. The exposed cells become rounded in shape and reduced in numbers as compared to untreated cells.

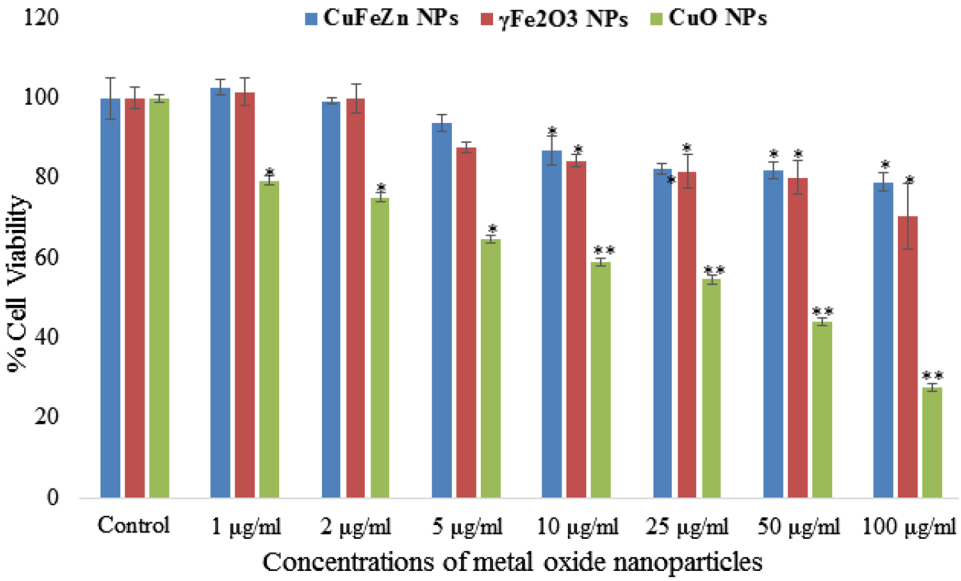

Fig. 3 Cytotoxicity assessment by MTT Assay in MCF-7 cells exposed to various concentrations (1–100 µg/ml) of CuFeZn-NPs, γFe_2O_3 and CuONPs for 24 h. Values are mean ± SE of three independent experiments. *p < 0.05, ** p < 0.01

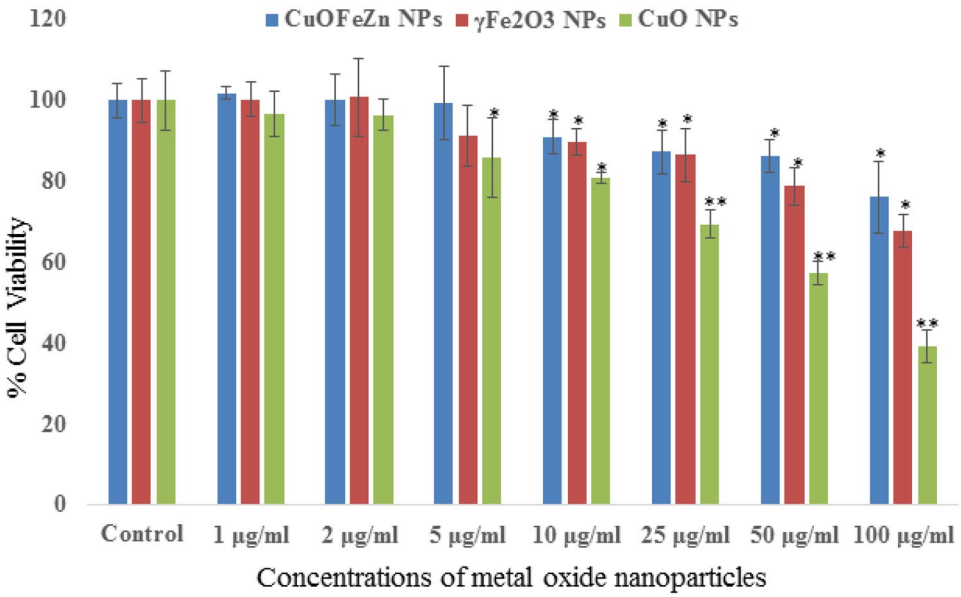

Fig. 4 Cytotoxicity assessments by NRU Assay in MCF-7 cells exposed to various concentrations (1–100 µg/ml) of CuOFeZn NPs, γFe_2O_3 and CuONPs for 24 h. Values are mean ± SE of three independent experiments. *p < 0.05, ** p < 0.01

3.6 ROS Generation

The key results of the induction in ROS generation are shown in Fig. 6a, b. The MCF-7 cells exposed to CuOFeZn NPs, γFe_2O_3NPs and CuONPs at 10, 25, and 50 µg/ml concentrations induced ROS production in a dose dependent manner. As shown in Fig. 6, an increase of 21% and 35% in CuOFeZn NPs, 41% and 61% in γFe_2O_3NPs and 54% and 89% in CuONPs was found in ROS production at 50 and 100 µg/ml, respectively.

3.7 MMP Level

The MMP level in MCF-7 cells was assessed after the exposure of CuOFeZn NPs, γFe_2O_3NPs and CuONPs for 24 h. As shown in Fig. 7a, b, a concentration dependent statistically significant ($p < 0.001$) decrease in MMP level was observed in MCF-7 cells. The reduction in MMP level was found to be 14% and 24% in CuOFeZn NPs, 37% and 46% in γFe_2O_3 and 52% and 58% in CuONPs at 25 and 50 µg/ml, respectively.

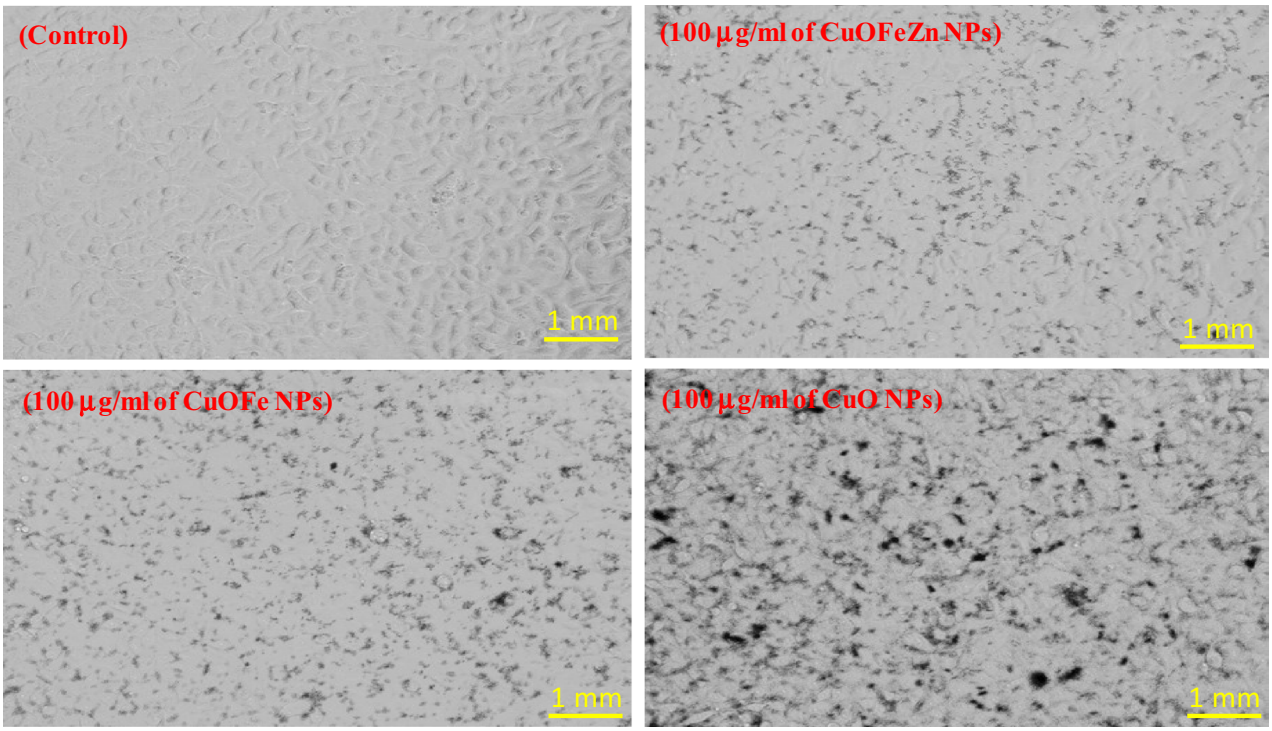

Fig. 5 Representative images of morphological changes in MCF-7 cells following the exposure of CuOFeZn NPs, γFe_2O_3 and CuO NPs for 24 h. Images were taken under the phase contrast inverted microscope at 20× magnification. Each scale bar = 1 mm

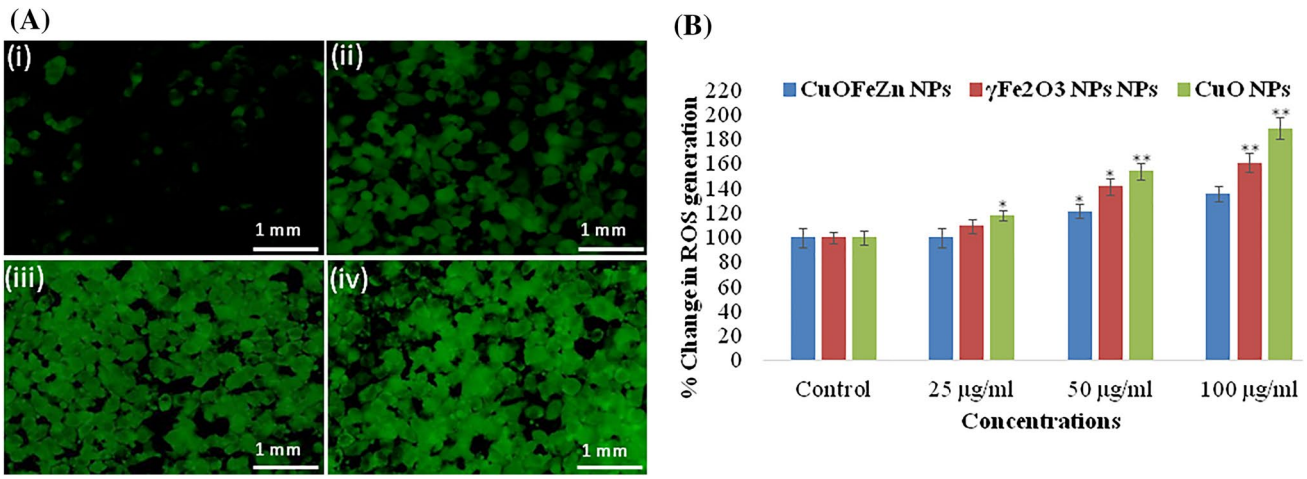

Fig. 6 **a** Representative images of induction in ROS generation in MCF-7 cells. ROS generation was studied using dichlorofluorescin-diacetate (DCFH-DA) dye after the exposure at 100 µg/ml for 24 h. (i) Control, (ii) CuOFeZn NPs, (iii) γFe_2O_3 and (iv) CuO NPs. **b** Percentage induction of ROS generation in MCF-7 cells following the exposure of various concentrations of CuOFeZn NPs, γFe_2O_3 and CuO NPs for 24 h. *p < 0.01, **p < 0.001 vs control. Each scale bar = 1 mm

4 Discussion

The increasing development of the nanotechnology manufacturing has headed to the large-scale production and application of engineered nanoparticles (NPs) [45]. Metal oxide nanoparticles are widely being used in various consumer products such as sun screen, cosmetics, textiles, food products, and medicines [46]. Due to their large surface area, high reactivity and small size the engineered nanomaterials may turn into an effective substance when manufactured as nanoparticles [47]. It is well known that they can reach to several organs such as brain, kidney, spleen, liver and heart through inhalation and absorption

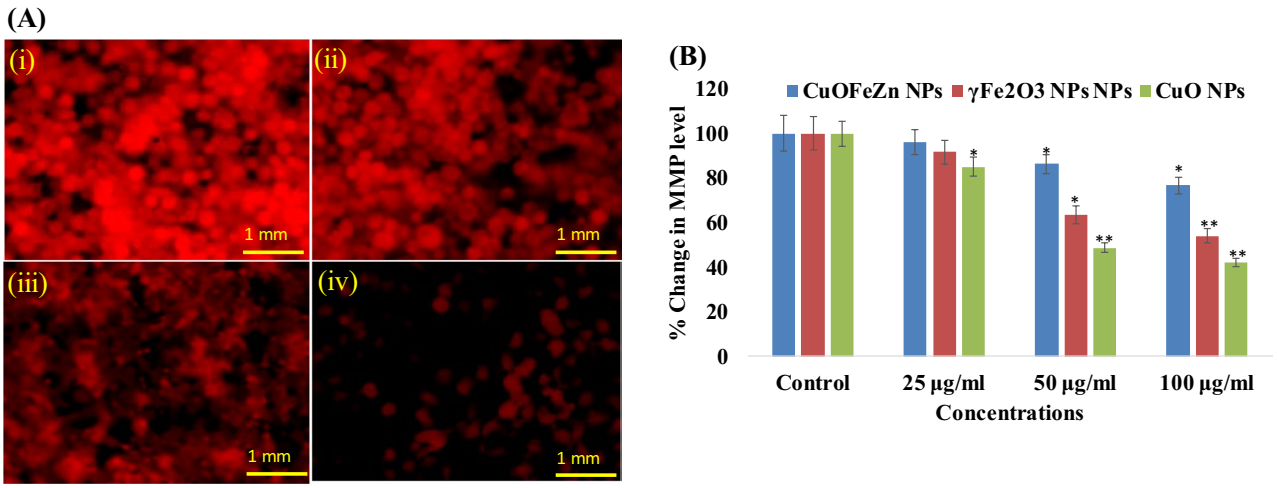

Fig. 7 **a** Representative images of reduction in the intensity of mitochondrial membrane potential (MMP) in MCF-7 cells exposed at 100 µg/ml for 24 h. MMP was studied using Rh123 fluorescent dye. (i) Control; (ii) CuOFeZn NPs, (iii) γFe_2O_3, and (iv) CuONPs. **b** Percentage induction in MMP level in MCF-7 cells after the exposure of different concentrations of CuOFeZn NPs, γFe_2O_3 and CuONPs. *p < 0.01, **p < 0.001 vs control. Each scale bar = 1 mm

[48]. Nanoparticles absorbed in the systemic circulation depend on their physicochemical properties migration to distant locations is a key concern in respect to their potential toxicity [49]. Therefore, this study was aimed to investigate potential cytotoxic responses of copper oxide nanoparticles (CuONPs), iron oxide nanoparticles (γFe_2O_3NPs) alone and with mixture of iron and zinc nanoparticles (CuOFeZn) in order to their biological responses on MCF-7, a human breast adenocarcinoma cell line. We have employed MTT and NRU colorimetric assays for the assessment of cytotoxicity of these NPs after the exposure of 24 h. The MTT and NRU results revealed a significant dose dependent cytotoxicity induced by CuOFeZnNPs, γFe_2O_3NPs and CuONPs in MCF-7 cells at 1–100 µg/ml. These results are in well agreement to the previously reported cytotoxic response of these NPs in this range [50]. Our results showed differential cytotoxic responses of different nanoparticles in MCF-7 cells that might be due to the method of preparation used, structure and size of the nanomaterials [51]. The impact of these nanoparticles on the cytotoxicity of MCF-7 cells could be due to differences in the characteristics and functions of the nanoparticles [52]. In order to explore the mechanism of the cytotoxicity cause by these NPs, we have studied the production of reactive oxygen species and integrity of mitochondrial membrane potential in MCF-7 after 24 h exposure. Production of ROS due to the nanoparticle's exposure is generally considered as a key role in the cytotoxicity and apoptosis. It is known that ROS can disturb the function of cells by directly acting on cell components such as, DNA, protein, lipids destroying their structure, which leads to cell death [53]. In present study, intracellular production of ROS was measured using DCF-DA fluorescence assay. Our results showed that CuOFeZn NPs, γFe_2O_3 and CuONPs produced ROS in MCF-7 cells in a dose dependent manner. These findings are very well supported by the reported literature which showed the cytotoxicity induced by different nanoparticles due to the increase in ROS production and oxidative stress [53–55]. We further assessed the integrity of mitochondrial membrane in MCF-7 cells after the exposure of CuOFeZn NPs, γFe_2O_3 and CuONPs. Our results showed that higher concentrations, i.e. 50 and 100 µg/ml of CuOFeZn NPs, γFe_2O_3 and CuONPs significantly decrease mitochondrial membrane potential in terms of reduction in fluorescence intensity of Rh123 in MCF-7 cells. It has also been reported that mitochondria are involved in the regulation of apoptosis. This reduction in the intensity of MMP level may activate the release of apoptogenic factors from mitochondria into the cytosol, which further leads to the death of MCF-7 cells [56, 57]. Consequently, it can be determined that the mechanism of cell death induced by CuOFeZn NPs, γFe_2O_3 and CuONPs in MCF-7 cells was attributed to the increased ROS production and the loss of mitochondrial membrane potential. In this continuation, the reactive oxygen species (ROS) which is responsible for to check the free radicals activities in cells were examined and it reveals that similar observation as the viability test and reveals that the single oxides (~ 50 nm) particles express a high intensity of green fluorescence DCF dye as compared to mixed/multi metal oxides in presence of untreated control. The reduction in MMP level in cancer cells with single and multi-metal oxide nanoparticles again shows significance of nanostructures.

The core of present work illustrates that at initial we have prepared the single and multi-metal oxide nanoparticles with the use of various chemicals such as copper acetate monohydrate, iron nitrate nonahydrate, zinc acetate di-hydrate and for the mixed metal oxide all these were mixed with different chemical conditions. The prepared single (CuO) and multi-metal oxides nanostructures were characterized with XRD, which shows that all the prepared nanoparticles are pure and high crystalline in character with different sized particles. The structural assessment of single and multi-metal oxide nanoparticles were checked with SEM and it reveals that the obtained images shows a sequential data's of spherical shaped nanoparticles ranges from 45 to 50 nm (single metal oxide, CuO and γFe_2O_3) and 80 nm (mixed metal oxide) nanoparticles. Including the basis characterization of two single and mixed metal oxide nanoparticles, prepared NPs efficacy were checked against breast cancer cells (MCF-7) consequently at dose dependent manner. The viability of cancer cells were measured via the MTT and NRU assays, and achieved data reveals that small sized or single metal oxides (CuO and γFe_2O_3NPs) are more feasible and potent as likened to bigger or mixed sized nanoparticles. The particles exhibit capability to enter easily in cells and possible to damage their organelles, due to lower density factor, whereas mixed/multi metal oxides have giant particles and exhibit higher density with low reactivity.

5 Conclusion

In conclusion, our results demonstrated that the synthesized single and multi-metal oxides nanoparticles (CuO, γFe_2O_3 and $CuZnFe_2O_3$) induced cytotoxicity in MCF-7 cells. The MTT and NRU assays showed a concentration dependent decrease in cell viability of MCF-7 cells. The results also showed that these nanoparticles are capable to induced ROS generation in MCF-7 cells which are responsible for the loss of mitochondrial membrane potential. The alterations in the morphology of MCF-7 cells induced by nanoparticles clearly exhibited cell death. These data established the utilization of nanomaterials against MCF-7 cells.

For the cancer treatment till to date a number of therapies were employed for the complete eradication of cancer cells for instance chemotherapy, radiotherapy etc. From these techniques the obtained results are not up to the mark because any cells remain again grow and form more cells. Also the surgical techniques are very costly and tedious for the poor patients and therefore a detailed work needs to establish for a successful therapy, which can cure well, efficiently at low price. The material science provides a great contribution in cancer studies also fulfil the cost effective ways to control and cure the cancers. Due to the biocompatible nature and easy handling process of synthesized material facilitates better and significant improvements with compared to the available technologies and have no any adverse effect, if used in permissible limit. The small dimension and high surface properties of the nanomaterials exhibit the property to enter directly in to the cells, which quickly reach to the cells organelles (DNA, RNA, endo plasmic reticulum etc.) as compared to the available drugs. The nanostructured materials against cancer studies will reduce the cost of the drugs also minimize the fear against surgery for deprived patents.

Acknowledgements The authors are grateful to the Deanship of Scientific Research, King Saud University for funding through Vice Deanship of Scientific Research Chairs.

Compliance with Ethical Standards

Conflict of interest The authors declare that they have no known competing financial interests or personal relationships that could have appeared to influence the work reported in this paper.

Research Involving Human and Animal Rights Also here declare that we haven't used any human or animal object except cell lines.

References

1. R.P. Andres, R.S. Averback, W.L. Brown et al., Research opportunities on clusters and cluster-assembled materials—a Department of Energy, Council on Materials Science Panel Report. J Mater Res **4**(3), 704–736 (1989)
2. V.F. Puntes, K.M. Krishnan, A.P. Alivisatos, Colloidal nanocrystal shape and size control: the case of cobalt. Science **291**, 2115–2117 (2001)
3. R.P. Andres, T. Bein, M. Dorogi et al., Coulomb staircase at room temperature in a self-assembled molecular nanostructure. Science **272**, 1323–1325 (1996)
4. C.B. Murray, C.R. Kagan, M.G. Bawendi, Self-organization of CdSe nanocrystallites into three-dimensional quantum dot superlattices. Science **270**, 1335–1338 (1995)
5. R. Cai, Y. Du, D. Yang, G. Jia, B. Zhu, B. Chen, Y. Lyu, K. Chen, D. Chen, W. Chen, L. Yang, Y. Zhao, Z. Chen, W. Tan, Free-standing 2D nanorafts by assembly of 1D nanorods for biomolecule sensing. Nanoscale **11**, 12169–12176 (2019)
6. M.J. Mayo, R.W. Siegel, A. Narayanasamy et al., Mechanical properties of nanophase TiO_2 as determined by nanoindentation. J. Mater. Res. **5**, 1073–1082 (1990)
7. M. Guermazi, H.J. Höfler, H. Hahn et al., Temperature dependence of the hardness of nanocrystalline titanium dioxide. J. Am. Ceram. Soc. **74**(10), 2672–2674 (1991)
8. Y. Mao, T.J. Park, F. Zhang et al., Environmentally friendly methodologies of nanostructure synthesis. Small **3**, 1122–1139 (2007)
9. Y. Yin, A.P. Alivisatos, Colloidal nanocrystal synthesis and the organic–inorganic interface. Nature **437**, 664–670 (2005)
10. F.X. Red, K.S. Cho, C.B. Murray et al., Three-dimensional binary super lattices of magnetic nanocrystals and semiconductor quantum dots. Nature **423**, 968–971 (2003)
11. S. Kinge, M. Crego-Calama, D.N. Reinhoudt, Self-assembling nanoparticles at surfaces and interfaces. Chem. Phys. Chem. **9**, 20–42 (2008)

12. K.E. Shopsowitz, H. Qi, W.Y. Hamad et al., Free-standing mesoporous silica films with tunable chiral nematic structures. Nature **468**, 422–425 (2010)
13. S. Sun, C.B. Murray, Synthesis of monodisperse cobalt nanocrystals and their assembly into magnetic superlattices. J. Appl. Phys. **85**, 4325–4330 (1999)
14. V.N. Rao, N.L. Reddy, M.M. Kumari, P. Ravi, M. Sathish, K.M. Kuruvilla, V. Preethi, K.R. Reddy, N.P. Shettie, T.M. Aminabhavi, M.V. Shankara, Photocatalytic recovery of H_2 from H_2S containing wastewater: Surface and interface control of photoexcitons in $Cu_2S@TiO_2$ core-shell nanostructures. Appl. Catal. B Environ. **254**, 174–185 (2019)
15. P.S. Basavarajappa, B.N.H. Seethya, N. Ganganagappa, K.B. Eshwaraswamy, R.R. Kakarla, Enhanced photocatalytic activity and biosensing of gadolinium substituted $BiFeO_3$ nanoparticles. Chem. Select. **3**, 9025–9033 (2018)
16. N.P. Shetti, S.D. Bukkitgar, K.R. Reddy, C.V. Reddy, T.M. Aminabhavi, ZnO-based nanostructured electrodes for electrochemical sensors and biosensors in biomedical applications. Biosensors Bioelectron. **141**, 111417 (2018)
17. C.V. Reddy, I.N. Reddy, K.R. Reddy, S. Jaesool, Yoo K, Template-free synthesis of tetragonal Co-doped ZrO_2 nanoparticles for applications in electrochemical energy storage and water treatment. Electrochim. Acta **317**, 416–426 (2019)
18. N.P. Shetti, S.J. Malode, D.S. Nayak, G.B. Bagihalli, S.S. Kalanur, R.S. Malladi, C.V. Reddy, T.M. Aminabhavi, K.R. Reddy, Fabrication of ZnO nanoparticles modified sensor for electrochemical oxidation of methdilazine. Appl. Surf. Sci. **496**, 143656 (2019)
19. N.P. Shetti, S.D. Bukkitgar, K.R. Reddy, C.V. Reddy, T.M. Aminabhavi, Nano structured titanium oxide hybrids-based electrochemical biosensors for healthcare applications. Colloids Surf. B Biointerfaces **178**, 385–394 (2019)
20. N.R. Reddy, U. Bhargav, M.M. Kumari, K.K. Cheralathan, M.V. Shankar, K.R. Reddy, T.A. Saleh, T.M. Aminabhavi, Highly efficient solar light-driven photocatalytic hydrogen production over Cu/FCNTs-titania quantum dots-based heterostructures. J. Environ. Manag. **254**, 109747 (2020)
21. K.R. Reddy, B.C. Sin, C.H. Yoo, W. Park, K.S. Ryu, J.S. Lee, D. Sohn, Y. Lee, A new one-step synthesis method for coating multiwalled carbon nanotubes with cuprous oxide nanoparticles. Scr. Mater. **58**(11), 1010–1013 (2008)
22. C.V. Reddya, I.N. Reddy, B. Akkinepally, K.R. Reddy, S. Jaesool, Synthesis and photoelectrochemical water oxidation of (Y, Cu) codoped α-Fe_2O_3 nano structure photoanode. J. Alloys Compd. **814**, 152349 (2020)
23. C.V. Reddy, I.N. Reddy, V.V.N. Harish, K.R. Reddy, N.P. Shetti, J. Shim, T.M. Aminabhavi, Efficient removal of toxic organic dyes and photoelectrochemical properties of iron-doped zirconia nanoparticles. Chemosphere **239**, 124766 (2020)
24. S.B. Patil, P.S. Basavarajappa, N. Ganganagappa, M.S. Jyothi, A.V. Raghu, K.R. Reddy, Recent advances in non-metals-doped TiO_2 nanostructured photocatalysts for visible-light driven hydrogen production, CO_2 reduction and air purification. Int. J. Hydrogen Energy **44**(26), 13022–13039 (2019)
25. R. Gholami, R. Ansari, Grain size and nanoscale effects on the nonlinear pull-in instability and vibrations of electrostatic actuators made of nanocrystalline material. Mater. Res. Express **5**(1), 015012 (2018)
26. N. Xia, N. Li, W. Rao, J. Yu, Q. Wu, L. Tan, H. Li, L. Gou, P. Liang, L. Li, X. Meng, Multifunctional and flexible ZrO_2-coated EGaIn nanoparticles for photothermal therapy. Nanoscale **11**, 10183–10189 (2019)
27. P. Sharma, S. Pant, V. Dave, K. Tak, V. Sadhu, K.R. Reddy, Green synthesis and characterization of copper nanoparticles by *Tinospora cardifolia* to produce nature-friendly copper nano-coated fabric and their antimicrobial evaluation. J. Microbiol. Methods **160**, 107–116 (2019)
28. R. Boppana, S.Y. Raut, G.K. Mohan, B. Sa, S. Mutalik, K.R. Reddy, K.K. Das, M.S. Biradar, R.V. Kulkarni, Novel pH-sensitive interpenetrated network polyspheres of polyacrylamide-g-locust bean gum and sodium alginate for intestinal targeting of ketoprofen: In vitro and in vivo evaluation. Colloids Surf. B Biointerfaces **180**, 362–370 (2019)
29. M. Sharma, A. Deohra, K.R. Reddy, V. Sadhu, Biocompatible in-situ gelling polymer hydrogels for treating ocular infection, in *Methods in Microbiology; Nanotechnology* (Elsevier, Amsterdam, 2019), pp. 93–114
30. A. Misra, S. Jain, D. Kishore, V. Dave, K.R. Reddy, V. Sadhu, J. Dwivedi, S. Sharma, A facile one pot synthesis of novel pyrimidine derivatives of 1,5-benzodiazepines via domino reaction and their antibacterial evaluation. J. Microbiol. Methods **163**, 105648 (2019)
31. S.B. Patil, S.Z. Inamdar, K.K. Das, K.G. Akamanchi, A.V. Patil, A.C. Inamadar, K.R. Reddy, A.V. Raghu, R.V. Kulkarni, Tailormade electrically-responsive poly (acrylamide)-graft-pullulan copolymer based transdermal drug delivery systems: synthesis, characterization, in-vitro and ex-vivo evaluation. J. Drug Deliv. Sci. Technol. **56**(A), 101525 (2020)
32. V. Dave, K. Tak, A. Sohgaura, A. Gupta, V. Sadhu, K.R. Reddy, Lipid-polymer hybrid nanoparticles: synthesis strategies and biomedical applications. J. Microbiol. Methods **160**, 130–142 (2019)
33. M. Moradi, M. Abdolhosseini, A. Zarrabi, B. Johari, A review on application of nano-structures and nano-objects with high potential for managing different aspects of bone malignancies. Nano-Struct. Nano-Obj. **19**, 100348 (2019)
34. S. Gulla, D. Lomada, V.V.S.S. Srikanth, M.V.K. Shankar, K.R. Reddy, S. Soni, M.C., Recent advances in nanoparticles-based strategies for cancer therapeutics and antibacterial applications, in *Methods in Microbiology*, vol. 46 (Academic Press, New York, 2019), pp, 255–293
35. S. Stanki, S. Suman, F. Haque et al., Pure and multi metal oxide nanoparticles: synthesis, antibacterial and cytotoxic properties. J. Nanobiotechnol. **14**, 73 (2016)
36. V.S. Shanthala, S.N.S. Devi, M.V. Murugendrappa, Synthesis, characterization and DC conductivity studies of polypyrrole/copper zinc iron oxide nanocomposites. J. Asian Ceram. Soc. **5**, 227–234 (2017)
37. R. Magaye, J. Zhao, L. Bowman et al., Genotoxicity and carcinogenicity of cobalt-nickel- and copper-based nanoparticles. Exp. Ther. Med. **4**, 551–561 (2012)
38. G. Sudlow, D.J. Birkett, D.N. Wade, The characterization of two specific drug binding sites on human serum albumin. Mol. Pharmacol. **11**, 824–832 (1975)
39. K. Aidas, J.M.H. Olsen, J. Kongsted et al., Photoabsorption of acridine yellow and proflavin bound to human serum albumin studied by means of quantum mechanics/molecular dynamics. J. Phys. Chem. **117**, 2069–2080 (2013)
40. F. Samari, M. Shamsipur, B. Hemmateenejad, Investigation of the interaction between amodiaquine and human serum albumin by fluoresence spectroscopy and molecular modeling. Eur. J. Med. Chem. **54**, 255–263 (2012)
41. M.A. Siddiqui, G. Singh, M.P. Kashyap et al., Influence of cytotoxic doses of 4-hydroxynonenal on selected neurotransmitter receptors in PC-12 cells. Toxicol. In Vitro **22**, 1681–1688 (2008)
42. M.A. Siddiqui, M.P. Kashyap, V. Kumar et al., Protective potential of trans-resveratrol against 4-hydroxynonenal induced damage in PC12 cells. Toxicol. In Vitro **24**, 1592–1598 (2010)
43. M.A. Siddiqui, Q. Saquib, M. Ahamed et al., Molybdenum nanoparticles-induced cytotoxicity, oxidative stress, G2/M arrest, and DNA damage in mouse skin fibroblast cells (L929). Colloids Surf. B **125**, 73–81 (2015)

44. M.A. Siddiqui, J. Ahmad, N.N. Farshori et al., Rotenone-induced oxidative stress and apoptosis in human liver HepG2 cells. Mol. Cell. Biochem. **384**(1–2), 59–69 (2013)
45. I. Khan, K. Saeed, I. Khan, Nanoparticles: properties, applications and toxicities. Arab. J. Chem. (2017). https://doi.org/10.1016/j.arabjc.2017.05.011
46. G. Dharanivasan, S. Sithanantham, M. Kannan et al., Metal oxide nanoparticles assisted controlled release of synthetic insect attractant for effective and sustainable trapping of fruit flies. J. Clust. Sci. **28**(4), 2167–2183 (2017)
47. M.A. Gatoo, S. Naseem, M.Y. Arfat et al., Physicochemical properties of nanomaterials: implication in associated toxic manifestations. BioMed. Res. Int. **498420**, 1–8 (2014)
48. H. Bahadar, F. Maqbool, K. Niaz et al., Toxicity of nanoparticles and an overview of current experimental models. Iran. Biomed. J **20**(1), 1 (2016)
49. Y. Zhang, Y. Bai, J. Jia et al., Perturbation of physiological systems by nanoparticles. Chem. Soc. Rev. **43**(10), 3762–3809 (2014)
50. C. Shen, S.A. James, M.D. DeJonge et al., Relating cytotoxicity, zinc ions, and reactive oxygen in ZnO nanoparticle–exposed human immune cells. Toxicol. Sci. **136**(1), 120–130 (2013)
51. S.K. Sohaebuddin, P.T. Thevenot, D. Baker et al., Nanomaterial cytotoxicity is composition, size, and cell type dependent. Part. Fibre Toxicol. **7**(1), 22 (2010)
52. I. Pujalté, I. Passagne, B. Brouillaud et al., Cytotoxicity and oxidative stress induced by different metallic nanoparticles on human kidney cells. Part. Fibre Toxicol. **8**(1), 10 (2011)
53. P. Khanna, C. Ong, B.H. Bay et al., Nanotoxicity: an interplay of oxidative stress, inflammation and cell death. Nanomaterials **5**(3), 1163–1180 (2015)
54. N. Li, C. Sioutas, A. Cho et al., Ultrafine particulate pollutants induce oxidative stress and mitochrondrial damage. Environ. Health. Perspect. **111**, 455–460 (2003)
55. P.P. Fu, Q. Xia, H.M. Hwang et al., Mechanisms of nanotoxicity: generation of reactive oxygen species. J. Food Drug Anal. **22**(1), 64–75 (2014)
56. G. Kroemer, L. Galluzzi, C. Brenner, Mitochondrial membrane permeabilization in cell death. Physiol. Rev. **87**, 99–163 (2007)
57. P. Vandenabeele, L. Galluzzi, T.V. Berghe et al., Molecular mechanisms of necroptosis: an ordered cellular explosion. Nat. Rev. Mol. Cell Biol. **11**, 700–714 (2010)